Available online at www.sciencedirect.com
ScienceDirect
Optics Communications 266 (2006) 456–464
OPTICS COMMUNICATIONS
www.elsevier.com/locate/optcom

Single frame blind image deconvolution by non-negative sparse matrix factorization

Ivica Kopriva [a,d,*], Dennis J. Garrood [b], Vesna Borjanović [b,c]

[a] Department of Electrical and Computer Engineering, The George Washington University, 801 22nd Street, NW, Washington, DC 20052, USA
[b] International Technology Center, 8100-120 Brownleigh Drive, Raleigh, NC 27617, USA
[c] Department of Applied Physics, Faculty of Electrical Engineering and Computing, University of Zagreb, Vukovarska 39, 10000 Zagreb, Croatia
[d] Department for Laser and Atomic Research Development, Institute Ruđer Bošković, P.O. Box 1016, 10001 Zagreb, Croatia

Received 19 December 2005; received in revised form 23 March 2006; accepted 5 May 2006

Abstract

Novel approach to single frame multichannel blind image deconvolution has been formulated recently as non-negative matrix factorization problem with sparseness constraints imposed on the unknown mixing vector that accounts for the case of non-sparse source image. Unlike most of the blind image deconvolution algorithms, the novel approach assumed no *a priori* knowledge about the blurring kernel and original image. Our contributions in this paper are: (i) we have formulated generalized non-negative matrix factorization approach to blind image deconvolution with sparseness constraints imposed on either unknown mixing vector or unknown source image; (ii) the criteria are established to distinguish whether unknown source image was sparse or not as well as to estimate appropriate sparseness constraint from degraded image itself, thus making the proposed approach completely unsupervised; (iii) an extensive experimental performance evaluation of the non-negative matrix factorization algorithm is presented on the images degraded by the blur caused by the photon sieve, out-of-focus blur with sparse and non-sparse images and blur caused by atmospheric turbulence. The algorithm is compared with the state-of-the-art single frame blind image deconvolution algorithms such as blind Richardson–Lucy algorithm and single frame multichannel independent component analysis based algorithm and non-blind image restoration algorithms such as multiplicative algebraic restoration technique and Van-Cittert algorithms. It has been experimentally demonstrated that proposed algorithm outperforms mentioned non-blind and blind image deconvolution methods.

PACS: 07.05.Pj; 42.30.Wb; 87.57.Gg; 42.69.Bz

Keywords: Image restoration; Blind deconvolution; Non-blind deconvolution; Non-negative sparse matrix factorization; Independent component analysis

1. Introduction

The goal of image deconvolution is to reconstruct the original image from an observation degraded by spatially invariant blurring process and noise. Neglecting the noise term the process is modeled as a convolution of a blurring kernel $h(s,t)$ with an original source image $f(x,y)$ as:

$$g(x,y) = \sum_{s=-K}^{K} \sum_{t=-K}^{K} h(s,t) f(x+s, y+t) \tag{1}$$

where K denotes the size of the blurring kernel. If the blurring kernel is known, a number of so-called non-blind algorithms is available to reconstruct original image $f(x,y)$ [1]. However, it is not always possible to measure or obtain information about the blurring kernel, which is why blind deconvolution (BD) algorithms are important. Comprehensive comparison of BD algorithms is given in [1]. They can be divided into those that estimate the blurring kernel $h(s,t)$ first and then restore original image by some of the

* Corresponding author. Tel.: +1 2029945508; fax: +1 2029945171.
E-mail address: ikopriva@gmail.com (I. Kopriva).

0030-4018/$ - see front matter © 2006 Elsevier B.V. All rights reserved.
doi:10.1016/j.optcom.2006.05.010

non-blind methods [1], and those that estimate the original image $f(x,y)$ and the blurring kernel simultaneously. In order to estimate the blurring kernel a support size has either to be given or estimated. Also, quite often *a priori* knowledge about the nature of the blurring process is assumed to be available in order to use appropriate parametric model of the blurring process [2]. It is not always possible to know the characteristic of the blurring process. Methods that estimate blurring kernel and original image simultaneously use either statistical or deterministic priors of the original image, the blurring kernel and the noise [2], which leads to a computationally expensive maximum likelihood estimation usually implemented by expectation maximization algorithm. In addition to that, exact distributions of the original image required by the maximum likelihood algorithm are usually unknown. One of the most representative algorithms from this class is the blind Richardson–Lucy (R–L) algorithm originally derived for non-blind deconvolution of astronomical images in [3,4], and later on formulated in [5] for BD and then modified by iterative restoration algorithm in [6]. This version of blind R–L algorithm is implemented in MATLAB© command *deconvblind*. It will be used in Section 3 for the comparison purpose during experimental performance evaluation of the to be introduced yet non-negative matrix factorization (NMF) based blind image deconvolution method. In order to overcome difficulties associated with the "standard" BD algorithms an approach was proposed in [7] based on quasi maximum likelihood with an approximate of the probability density function. It however assumed that original image has sparse or super-Gaussian distribution. This is generally not true because image distributions are mostly sub-Gaussian. To overcome that difficulty it was proposed in [7] to apply sparsifying transform to blurred image. However, design of such a transform requires knowledge of at least the typical class of images to which original image belongs in which case training data can be used to design sparsifying transform. Multivariate data analysis methods such as independent component analysis (ICA) [8] might be used to solve BD problem as a blind source separation (BSS) problem where unknown blurring process is absorbed into what is known as a mixing matrix. The advantage of the ICA approach would be that no *a priori* knowledge about the origin and size of the support of the blurring kernel is required. However, multi-channel image required by ICA is not always available. Even if it is, it would require the blurring kernel to be non-stationary, which is true for the blur caused by atmospheric turbulence [9], but it is not true for the out-of-focus blur for example. Therefore, an approach to single frame multi-channel blind deconvolution that requires minimum of *a priori* information about blurring process and original image would be of great interest. Single frame multi-channel representation was proposed in [10]. It was based on a bank of 2D Gabor filters [11] used due to their ability to realize multi-channel filtering. ICA algorithms have been applied in [10] to multichannel image in order to extract the source image and two spatial derivatives along x and y directions. There is however critical condition that source image and their spatial derivatives must be statistically independent. In general this is not true as already observed in [12]. Consequently, quality of the image restoration by proposed single frame multi-channel approach depends on how well each particular image satisfies statistical independence assumption. Therefore, an extension of the ICA approach formulated in [10] is given in [13] where it has been shown that single frame multichannel BD can be formulated as NMF problem with sparseness constraints imposed on the unknown mixing vector. Consequently, no *a priori* knowledge about either the origin or the size of the blurring process is required. Because NMF is deterministic approach no *a priori* information about the statistical nature of the source image is required as well. We present here generalized NMF approach to blind image deconvolution with sparseness constraints imposed on either unknown mixing vector or unknown source image. The criteria are provided to distinguish whether source image was sparse or not as well as to estimate appropriate sparseness constraint from degraded image itself making the proposed approach completely unsupervised. The rest of the paper is organized as follows. We introduce briefly in Section 2 non-blind Van-Cittert [14] and multiplicative algebraic restoration technique (MART) [17,18] image restoration algorithms, blind R–L algorithm [5,6], ICA approach to single frame multichannel BD [10]. We describe in more details generalized NMF approach to single frame multichannel BD with sparseness constraints originally given in [13]. Comparative experimental performance evaluation is given in Section3 for images degraded by photon sieve, sparse and non-sparse images degraded by out-of-focus blur and images degraded by atmospheric turbulence. Conclusion is presented in Section 4.

2. Basic overview of the compared non-blind and blind image deconvolution algorithms

Before proceeding to description of the to be compared non-blind and blind image deconvolution algorithms we shall rewrite image observation model given by Eq. (1) in the lexicographical notation:

$$\mathbf{g} = \mathbf{H}\mathbf{f} \tag{2}$$

where $\mathbf{g}, \mathbf{f} \in Z_{0+}^{MN}$, $\mathbf{H} \in R_{0+}^{MN \times MN}$ assuming image dimensionality of $M \times N$ pixels. Observed image vector $\mathbf{g}$ and original image vector $\mathbf{f}$ are obtained by the row stacking procedure. The matrix $\mathbf{H}$ is block-circulant matrix [14], and it absorbs into itself the blurring kernel $h(s,t)$ assuming at least size of it, K, to be known.

2.1. Non-blind Van-Cittert and MART algorithms

Van-Cittert algorithm solves image restoration problem through the following iterative procedure [14]:

$$\hat{\mathbf{f}}^{(k+1)} = \hat{\mathbf{f}}^{k} + \varepsilon \mathbf{H}^{\mathrm{T}}(\mathbf{g} - \mathbf{H}\hat{\mathbf{f}}^{k}) \tag{3}$$

where k denotes iteration index and ε denotes small learning gain. It is assumed that blurring kernel $h(s,t)$ contained in the block-circulant matrix $\mathbf{H}$ is known. The MART algorithm is realized through the following multiplicative iteration scheme [17,18]:

$$\hat{\mathbf{f}}^{(k+1)} = \hat{\mathbf{f}}^{(k)} \otimes [(\mathbf{Hg}) \varnothing (\mathbf{H}^{\mathrm{T}}\mathbf{H}\hat{\mathbf{f}}^{(k)})] \tag{4}$$

where in Eq. (4) symbol $\otimes$ denotes component-wise multiplication and symbol $\varnothing$ denotes component-wise division. The MART algorithm also assumes knowledge of the blurring kernel $h(s,t)$. Multiplicative update rule (4) ensures positivity of the reconstructed image automatically what is an advantage of the MART algorithm over the Van-Cittert algorithm.

2.2. Blind R–L algorithm

Blind R–L method [5,6] follows from the non-blind version of the R–L method [3,4] which itself follows from Bayesian paradigm approach to statistical inference which dictates that inference about true image $\mathbf{f}$ should be based on conditional probability $P(\mathbf{f}|\mathbf{g})$ given by the Bayes rule. The prior knowledge about image degradation process is incorporated in probabilities $P(\mathbf{g}|\mathbf{f})$ and $P(\mathbf{f})$. These probabilities are also called *priors*. In the low light level imaging such as in astronomy, microscopy and the night vision imaging, the appropriate choice for $P(\mathbf{g}|\mathbf{f})$ is Poisson distribution [15,16]. In the high-brightness conditions the Poisson *prior* should be replaced by the Gaussian one. The R–L algorithm follows when non-informative *prior* is chosen for $P(\mathbf{f})$ i.e. $P(\mathbf{f}) \propto$ const. The algorithm is obtained through the maximization of the log-likelihood function:

$$\hat{\mathbf{f}} = \underset{\mathbf{f}}{\operatorname{argmax}} \log P(\mathbf{g}|\mathbf{f}) \tag{5}$$

EM algorithm is employed to solve problem (5) yielding numerically efficient multiplicative iterative algorithm known as blind R–L algorithm [5]:

$$\hat{\mathbf{H}}_{i+1}^{(k)} = [(\hat{\mathbf{f}}^{(k-1)})^{\mathrm{T}}(\mathbf{g} \varnothing (\hat{\mathbf{H}}_i^k \hat{\mathbf{f}}^{(k-1)}))]\hat{\mathbf{H}}_i^{(k)} \tag{6a}$$

$$\hat{\mathbf{f}}_{i+1}^{(k+1)} = \left[\hat{\mathbf{f}}_i^{(k)} \otimes \left(\mathbf{H}^{\mathrm{T}}\left(\mathbf{g} \varnothing \left(\mathbf{H}\hat{\mathbf{f}}_i^{(k)}\right)\right)\right)\right] \varnothing (\mathbf{H}^{\mathrm{T}}\mathbf{1}) \tag{6b}$$

where index i is used to denote internal iteration of the blind R–L algorithm, k denotes main iteration index and $\mathbf{1}$ denotes a column vector with all entries equal to 1. Multiplicative update rules (6a and 6b) ensure positivity of both blurring kernel and reconstructed image automatically. As we see from Eq. (6) the problem with blind R–L algorithm is that although the blurring kernel incorporated in the block-circulant matrix $\mathbf{H}$ is estimated from the observed image, the support size K, see Eq. (1), must be known or estimated by some method. This knowledge is not always available *a priori*. This is especially true for non-stationary degradation process such as atmospheric turbulence where the strength of the turbulence, measured by the parameter called scintillation index, will strongly influence the size of the blur.

2.3. ICA approach to single frame multichannel BD (SFMICA)

Single frame multi-channel representation was proposed in [10]. It was based on a bank of 2D Gabor filters [11] used due to their ability to realize multi-channel filtering and decomposing an input image into sparse images containing intensity variation over narrow range of frequency and orientation. Multichannel version of degraded image is shown in [10] to be in a form:

$$\mathbf{G} = \begin{bmatrix} \mathbf{g}^{\mathrm{T}} \\ \mathbf{g}_1^{\mathrm{T}} \\ \dots \\ \mathbf{g}_L^{\mathrm{T}} \end{bmatrix} \cong \begin{bmatrix} a_1 & a_2 & a_3 \\ a_{11} & a_{12} & a_{13} \\ \dots & \dots & \dots \\ a_{L1} & a_{L2} & a_{L3} \end{bmatrix} \begin{bmatrix} \mathbf{f}^{\mathrm{T}} \\ \mathbf{f}_{\mathbf{x}}^{\mathrm{T}} \\ \mathbf{f}_{\mathbf{y}}^{\mathrm{T}} \end{bmatrix} = \mathbf{AF} \tag{7}$$

where images $\boldsymbol{g}_l$, $l = 1,\dots,L$, are produced by Gabor filters, $\mathbf{f}$ represents source image and $\mathbf{f}_x$ and $\mathbf{f}_y$ represent spatial derivatives along x and y directions, respectively. Unknown elements a_{lm} of the mixing matrix absorb the blurring kernel assuming no *a priori* information about it including its size. The ICA algorithm has been applied in [10] to image model (7) in order to extract the source image $\mathbf{f}$. There is however critical condition for the source image that must hold in order for ICA algorithm to work. Image $\mathbf{f}$ and its spatial derivatives $\mathbf{f}_x$ and $\mathbf{f}_y$ must be statistically independent. This is in general not true as already observed in [12]. Consequently, quality of the image restored by proposed single frame multi-channel approach depends on how well each particular image satisfies statistical independence assumption.

2.4. NMF approach to single frame multichannel BD (SFMNMF)

It was further shown in [13] that single frame multichannel blind deconvolution can approximately be represented as:

$$\mathbf{G} = \begin{bmatrix} \mathbf{g}^{\mathrm{T}} \\ \mathbf{g}_1^{\mathrm{T}} \\ \dots \\ \mathbf{g}_L^{\mathrm{T}} \end{bmatrix} \cong \begin{bmatrix} \tilde{a}_1 \\ \tilde{a}_{21} \\ \dots \\ \tilde{a}_{L1} \end{bmatrix} [\mathbf{f}^{\mathrm{T}}] = \tilde{\mathbf{a}}\mathbf{f}^{\mathrm{T}} \tag{8}$$

where images $\boldsymbol{g}_l$, $l = 1,\dots,L$, were again produced by Gabor filters and coefficients of the unknown blurring kernel were absorbed into coefficients $\tilde{a}_{lm}$ of the unknown mixing vector $\tilde{\mathbf{a}}$. Image model (8) suggests the existence of only source image $\mathbf{f}$ in the linear image observation model. Spatially oriented Gabor filters produce images with sparse (super-Gaussian) distributions i.e. multichannel version $\mathbf{G}$ of the observed image $\mathbf{g}$ is mostly sparse. This gave motivation in [13] to formulate single frame multichannel blind image deconvolution problem as NMF problem with sparseness constraint. If the source image $\mathbf{f}$ is non-sparse i.e. sub-Gaussian, which is the case for natural images, an unknown mixing vector $\tilde{\mathbf{a}}$ must be sparse. This case has been

worked out in [13]. We present here generalized NMF approach to blind image deconvolution with sparseness constraints [19–21], imposed on either unknown mixing vector or unknown source image. We follow presentation given in [21,22], where NMF problem with sparseness constraints is formulated as:

$$D(\mathbf{G}\|\tilde{\mathbf{a}},\mathbf{f}) = \tfrac{1}{2}\left\|\mathbf{G}-\tilde{\mathbf{a}}\mathbf{f}^{\mathrm{T}}\right\|_F^2 + \alpha_{\tilde{\mathbf{a}}}J_{\tilde{\mathbf{a}}}(\tilde{\mathbf{a}}) + \alpha_{\mathbf{f}}J_{\mathbf{f}}(\mathbf{f}) \quad \text{s.t. } \tilde{a}_i \geqslant 0,\ f_j \geqslant 0\ \forall i,j \tag{9}$$

where $J_{\tilde{\mathbf{a}}}(\tilde{\mathbf{a}})$ and $J_{\mathbf{f}}(\mathbf{f})$ represent appropriate constraints and $\alpha_{\tilde{\mathbf{a}}}$ and $\alpha_{\mathbf{f}}$ are regularization factors. Constraints represent *a priori* knowledge we have about the unknown source image and mixing vector. Typical constraints are sparsity and smoothness. It is believed that these additional constraints enable to overcome difficulties associated with early NMF algorithms [20], which is poor performance in the blind source separation problems due to non-uniqueness of the solution and to help to extract physically meaningful sources in biomedical applications such as EEG and MEG [21,22]. We believe that from the same reasons NMF with sparseness constraints extract physically meaningful source image in BD problem. Due to the already discussed fact that multichannel version $\mathbf{G}$ of observed image $\mathbf{g}$ is sparse we shall impose sparseness constraints on either source image $\mathbf{f}$ or mixing vector $\tilde{\mathbf{a}}$. It has been already shown in the context of underdetermined blind source separation problem (more sources than sensors), Refs. [23,24], that l_1 norm is appropriate sparsity measure, which ensures reconstruction of the source signals. This justifies our choice for $J(\mathbf{x}) = \sum_n x_n$ where $\mathbf{x}$ is some nonnegative vector. Under this condition minimization of divergence $D(\mathbf{G}\|\tilde{\mathbf{a}},\mathbf{f})$ gives the following multiplicative update learning rules for $\tilde{\mathbf{a}}$ and $\mathbf{f}$ [21,22]:

$$\begin{aligned}\tilde{\mathbf{a}} &= \tilde{\mathbf{a}} \otimes [\mathbf{G}\mathbf{f} - \alpha_{\tilde{\mathbf{a}}}]_{\varepsilon} \oslash (\tilde{\mathbf{a}}\mathbf{f}^{\mathrm{T}}\mathbf{f} + \varepsilon)\\ \mathbf{f} &= \mathbf{f} \otimes ([\mathbf{G}^{\mathrm{T}}\tilde{\mathbf{a}} - \alpha_{\mathbf{f}}]_{\varepsilon} \oslash (\mathbf{f}\tilde{\mathbf{a}}^{\mathrm{T}}\tilde{\mathbf{a}} + \varepsilon))\end{aligned} \tag{10}$$

where again symbol '$\otimes$' denotes component-wise multiplication, symbol '$\oslash$' denotes component-wise division and $[x]_{\varepsilon} = \max(x,\varepsilon)$ with $\varepsilon = 10^{-9}$. In order to obtain truly unsupervised image restoration algorithm regularization factors $\alpha_{\tilde{\mathbf{a}}}$ and $\alpha_{\mathbf{f}}$, that we sometimes refer to as a sparseness constraints, have to be estimated from the multichannel image $\mathbf{G}$ only. We propose to use kurtosis of the degraded image $\mathbf{g}$ as a sparsity measure to distinguish whether original image $\mathbf{f}$ was sparse i.e. super-Gaussian or non-sparse i.e. sub-Gaussian. If $\kappa(\mathbf{g}) < 0$ we decide that source image was non-sparse and that, due to the fact that multichannel image $\mathbf{G}$ was sparse, the unknown mixing vector $\tilde{\mathbf{a}}$ must be sparse. In this case we set $\alpha_{\mathbf{f}} = 0$ and estimate $\alpha_{\tilde{\mathbf{a}}}$ from $\mathbf{G}$ as a ratio between number of sparse images L_s and overall number of images $L+1$, [13], i.e. $\alpha_{\tilde{\mathbf{a}}} = L_s/(L+1)$. To estimate $L_s$kurtosis κ of each image in $\mathbf{G}$ is estimated. Image $\mathbf{g}_l$, $l = 1,\ldots,L+1$, is considered to be sparse if $\kappa(\mathbf{g}_l) > 0$. If $\kappa(\mathbf{g}) > 0$ we decide that source image was sparse. In this case we set $\alpha_{\tilde{\mathbf{a}}} = 0$ and estimate $\alpha_{\mathbf{f}}$ from $\mathbf{G}$ as $\alpha_{\mathbf{f}} = \kappa(\mathbf{g})$. This enables to obtain truly unsupervised blind image deconvolution method able to restore both sparse and non-sparse images. Approach presented in [13] is not so general. Ability to restore sparse images is important for a number of applications where images are acquired under low-light-level conditions. For example, such scenarios arise in astronomy, microscopy, under-water imaging and night vision imaging. In order to impose the least level of *a priori* knowledge about the source image and mixing vector we start the learning process (10) with the random choice for both $\tilde{\mathbf{a}}$ and $\mathbf{f}$. Before proceeding to the comparative performance analysis of described blind and non-blind image deconvolution methods we want to analyze in more details behavior of the NMF approach to BD with respect to two basic problems in the image restoration: stability and uniqueness of the solution. We have already conjectured that sparseness constraint enables to obtain solution that is physically sensible. We want to analyze whether the learning rule (10) will converge toward similar (possibly same) local optimum from different randomly chosen initial conditions for $\tilde{\mathbf{a}}$ and $\mathbf{f}$. For this purpose we have calculated the mean square error (MSE) defined as:

$$e(k) = \sqrt{\frac{1}{MN}\sum_{n=1}^{MN}\left(\mathbf{f}_n^{\mathrm{ref}} - \mathbf{f}_n(k)\right)^2} \tag{11}$$

where k represents iteration index, n represents pixel index and $\mathbf{f}^{\mathrm{ref}}$ is image reconstructed first time. We have calculated MSE error for 100 runs. Each reconstructed image was normalized to an 8-bit resolution such that MSE error is expressed in a number of bits. Fig. 1 shows results of described analysis where an image degraded by photon sieve placed in front of the CCD sensor, which is shown in Fig. 2, was used for testing purpose. The SFMNMF reconstructed image $\mathbf{f}^{\mathrm{ref}}$ itself is shown in Fig. 7. NMF result together with the results of other algorithms is described in

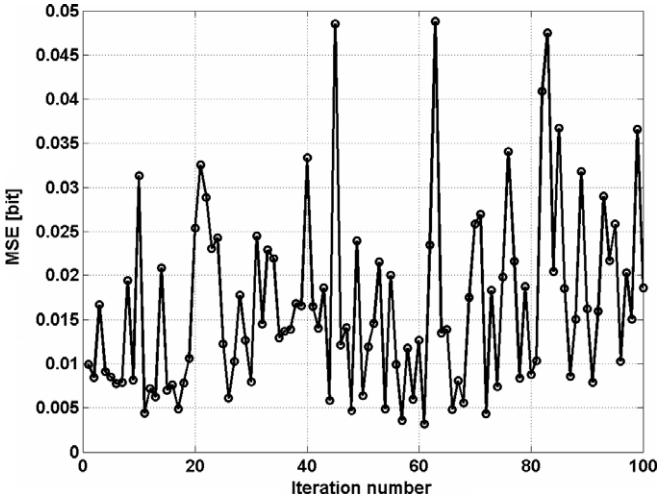

Fig. 1. MSE error with respect to reference image obtained by blind deconvolution of image shown in Fig. 2 and by using SFMNMF algorithm. Reference image is shown in Fig. 7. At each run initial conditions for mixing vector and source image were generated randomly.

Fig. 2. Image degraded by photon sieve.

Section 3. Restored images were obtained after 3 iterations when relative error criterion set 0.1% was satisfied. It can be seen that MSE error is always less than 0.05 bit which confirms that NMF algorithm with sparseness constraints indeed converges toward same physically sensible solution. Because the algorithm consistently produced results with such a small deviation it can be considered as a stable i.e. random perturbation in the initial conditions for mixing vector and source image gave always the restored images that look the same from the practical application point of view.

3. Experimental results

We show in Fig. 2 an image degraded by photon sieve placed in front of the CCD sensor. Image restored by the sparse version of the Van-Cittert algorithm is shown in Fig. 3 and is obtained after 5 iterations. Image restored by the sparse version of the MART algorithm is shown in Fig. 4 and is obtained after 50 iterations. Fig. 5 shows image restored by blind R–L algorithm obtained after 5 iterations with the circular blurring kernel with the radius of $R = 2$ pixels. Because the size of the blurring kernel must be known *a priori* for R–L algorithm the algorithm had to be run several times with the various values for the radius R and then the value that corresponded with the best quality of the restored image was chosen. This is time consuming process and it is not applicable in real time image enhancement. In addition to that, it is known that either underestimate or overestimate of the size of the blurring kernel leads to severe distortions of the images reconstructed by blind R–L algorithm and other blind algorithms of the similar type [1]. Fig. 6 shows image restored by SFMICA algorithm. FastICA algorithm with the tanh nonlinearity was used as in [10,25]. Fig. 6 shows image restored by described SFMNMF algorithm. Note very poor quality of the image restored by SFMICA algorithm due to the fact that assumption about statistical independence between source image $\mathbf{f}$ and its spatial derivatives $\mathbf{f}_x$ and $\mathbf{f}_y$ does not hold. Note also that SFMNMF algorithm produced restored image with the superior quality over the blind R–L algorithm and even non-blind sparse

Fig. 3. Image reconstructed by the modified Van-Cittert algorithm after 5 iterations.

Fig. 4. Image reconstructed by MART algorithm after 50 iterations.

Fig. 5. Image reconstructed by blind R–L algorithm after 5 iterations with the circular blurring kernel with the radius $R = 2$ pixels.

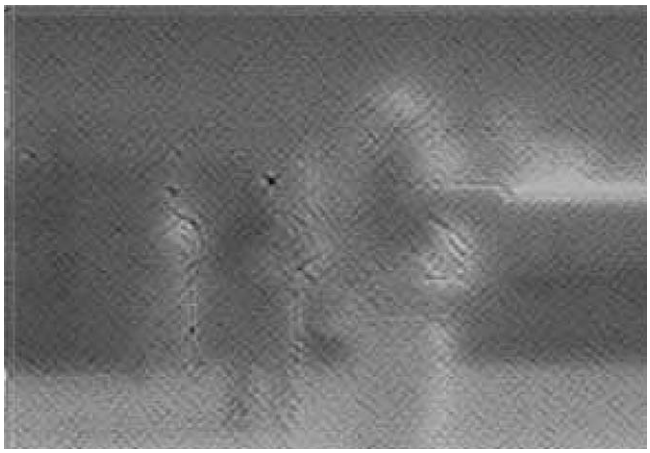

Fig. 6. Image reconstructed by the single frame multichannel ICA algorithm.

Fig. 7. Image reconstructed by the single frame multichannel NMF algorithm.

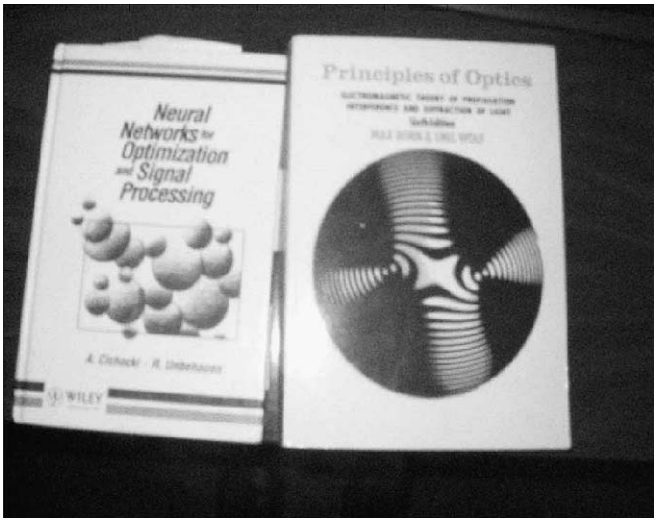

Fig. 8. Non-sparse (sub-Gaussian) image degraded by out-of-focus blur obtained by digital camera in manually de-focused mode.

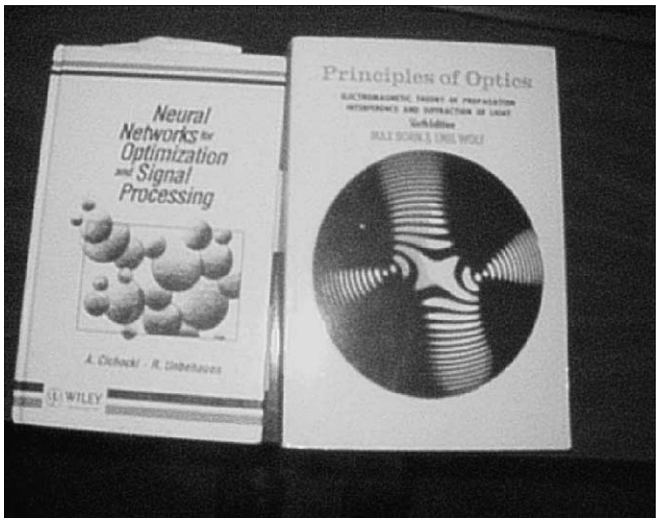

Fig. 9. Non-sparse image reconstructed by SFMNMF algorithm.

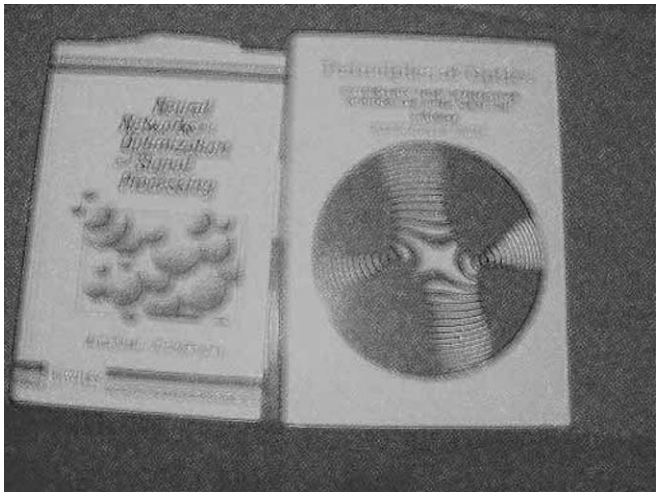

Fig. 10. Non-sparse image reconstructed by SFMICA algorithm.

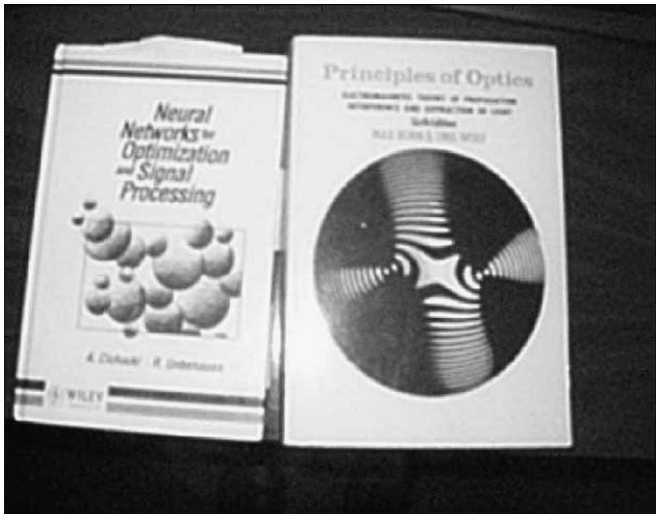

Fig. 11. Non-sparse image reconstructed by blind Richardson–Lucy algorithm after 5 iterations with the circular blurring kernel with radius of $R = 3$ pixels.

Van-Cittert and MART algorithms despite the fact that no information about the blurring process was used/required by the SFMNMF algorithm. Fig. 8 shows non-sparse (sub-Gaussian) blurred image obtained by digital camera in manually de-focused mode. Fig. 9 shows image reconstructed by SFMNMF algorithm. Because kurtosis of the blurred image was negative the sparseness constraint α_f has been set to zero. Sparseness constraint $\alpha_{\tilde{\mathbf{a}}}$ was estimated as 0.82. Images shown in Figs. 8 and 9 were already shown in [13]. Image reconstructed by SFMICA algorithm is shown in Fig. 10 where FastICA algorithm with tanh nonlinearity was used again. Image restored by the SFMICA algorithm has again poor quality due to the already discussed assumptions made on the statistical independence between source image and its spatial derivatives.

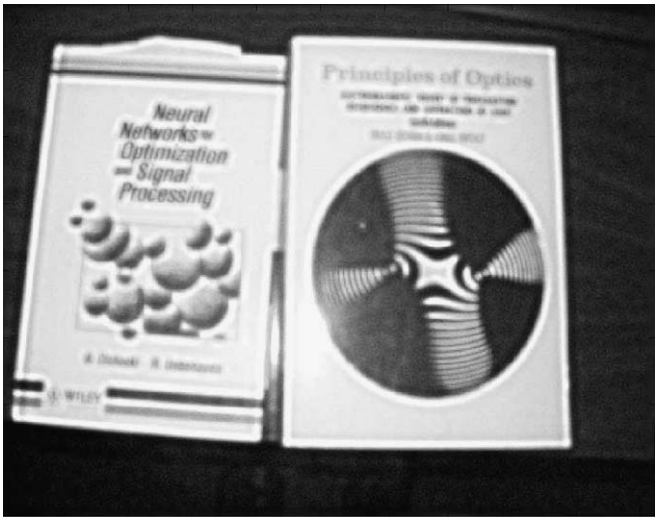

Fig. 12. Non-sparse image reconstructed by blind Richardson–Lucy algorithm after 5 iterations with the circular blurring kernel with radius of $R = 5$ pixels.

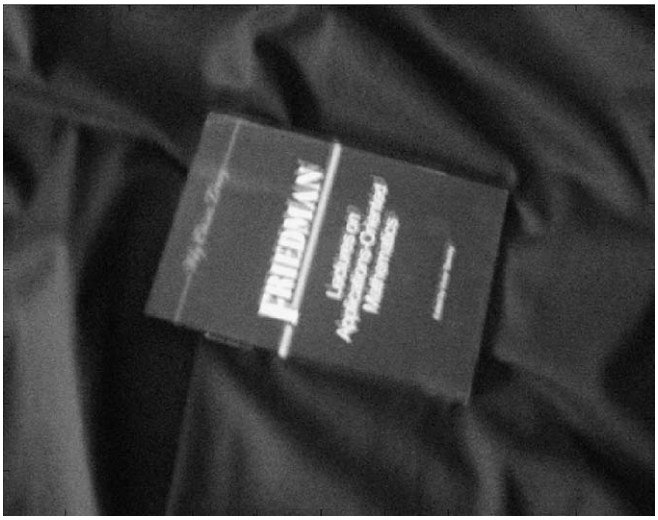

Fig. 13. Sparse (super-Gaussian) image degraded by out-of-focus blur obtained by digital camera in manually de-focused mode. Image has been acquired under low-light-level conditions.

Fig. 14. Sparse image reconstructed by SFMNMF algorithm.

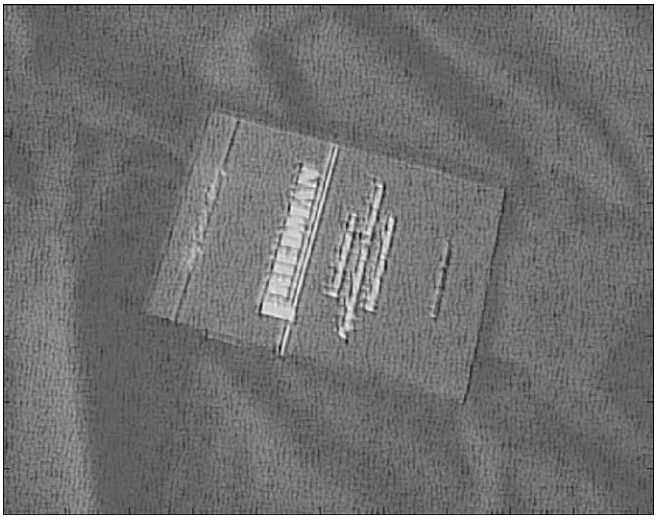

Fig. 15. Sparse image reconstructed by SFMICA algorithm.

Fig. 16. Sparse image reconstructed by blind Richardson–Lucy algorithm after 5 iterations with the circular blurring kernel with radius of $R = 3$ pixels.

The SFMNMF algorithm eliminates all these problems due to the fact that no *a priori* knowledge about either the size of the blurring kernel or statistical nature of the source image is required. Fig. 11 shows image restored by the blind R–L algorithm after 5 iterations with the circular blurring kernel and radius of $R = 3$ pixels. Because the blurred image, Fig. 8, was not highly de-focused blind R–L algorithm with the kernel size of $R = 3$ pixels produced good result but still inferior to this produced by SFMNMF algorithm shown in Fig. 9. Again, blind R–L algorithm had to be run several times for different values of the size of the blurring kernel R. Then, image with the best quality had to be chosen. In order to illustrate sensitivity of the blind R–L algorithm (and other methods of that type [1]) on the overestimation of the size of the blurring kernel we show in Fig. 12 image restored by the blind R–L algorithm with the kernel size of $R = 5$ pixels obtained after 5 iterations. In order to illustrate performance of described SFMNMF algorithm for the blurred images acquired under low-light-level conditions, which are sparse i.e. super-Gaussian, we have recorded blurred image obtained by digital camera in manually de-focused mode under described conditions. It is shown in Fig. 13. Fig. 14 shows image reconstructed by SFMNMF algorithm. Because kurtosis of the blurred image was positive the regularization parameter $\alpha_{\tilde{\mathbf{a}}}$ has been set to zero. Regularization parameter $\alpha_{\mathbf{f}}$ was estimated as $\kappa(\mathbf{g}) = 7.588$. Image reconstructed by SFMICA algorithm is shown in Fig. 15 where FastICA algorithm with tanh nonlinearity was used again. Image restored by the SFMICA algorithm has again poor quality due to the already discussed assumptions made on the statistical independence between source image and its spatial derivatives. Again, the SFMNMF algorithm eliminates all these problems due to the fact that no *a priori* knowledge about either the size of the blurring kernel or statistical nature of the source image is required. Fig. 16 shows image restored by the blind R–L algorithm after 5 iterations with the circular blurring kernel and radius of $R = 3$ pixels. Because the blurred image, Fig. 13, was not highly de-focused blind R–L algorithm with the kernel size of $R = 3$ pixels produced good result but still inferior to this produced by SFMNMF algorithm shown in Fig. 14. Again, blind R–L algorithm had to be run several times for different values of the size of the blurring kernel R. Then, image with the best quality had to be chosen. Fig. 17 shows randomly selected frame taken from the image sequence of the Washington monument obtained in the conditions of the weak atmospheric turbulence [9]. Image was deconvolved by the SFMNMF algorithm, SFMICA algorithm with the JADE method used to implement ICA [26] and blind R–L algorithm. Canny's edge detector was applied on deconvolved images with the results shown in Fig. 18. From left to right are: blurred image, SFMNMF restored image, SFMICA restored image and blind R–L restored images with the Gaussian

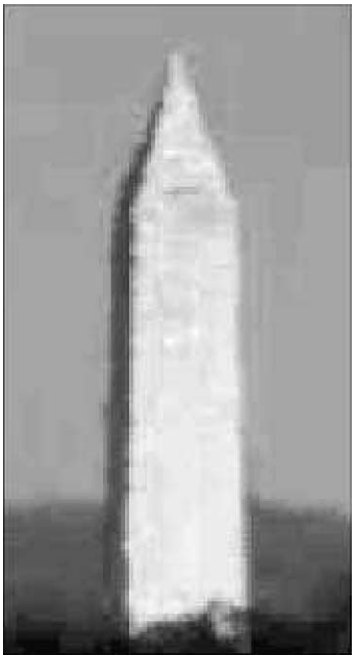

Fig. 17. Picture of the Washington monument obtained in the conditions of the weak atmospheric turbulence [9].

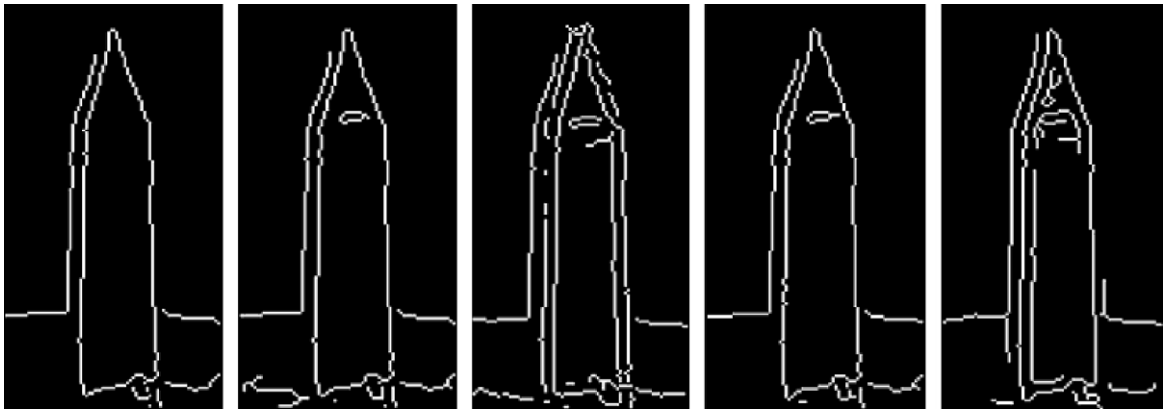

Fig. 18. Edges detected by Canny's edge detector. From left to right: Blurred image, SFMNMF restored image, SFMICA restored image, blind R–L algorithm with $R = 3$ and SIGMA = 3 pixels, blind R–L algorithm with $R = 5$ and SIGMA = 5 pixels.

type of the blurring kernel (suitable for modeling atmospheric turbulence) with the radius of $R = 3$ and standard deviation SIGMA = 3 pixels and $R = 5$ and SIGMA = 5 pixels. It can be observed that windows, which are present on the Washington monument, are not reconstructed on the blurred image. It can be also observed that SFMICA produced poor results due to already discussed reasons. Blind R–L algorithm with parameters $R = 3$ and SIGMA = 3 produced result of the quality which is comparable with those obtained by the SFMNMF algorithm (only some details in the background are missed by the blind R–L algorithm), while blind R–L algorithm with parameters $R = 5$ and SIGMA = 5 produced result with the very poor quality illustrating again the known sensitivity of the blind R–L method on either overestimation or underestimation of the size of the blurring kernel.

4. Conclusion

Non-negative sparse matrix factorization approach to single frame blind image deconvolution has been formulated. The main property of the algorithm is that no *a priori* knowledge about the statistical nature of the source image as well as about origin or size of the blurring kernel is required. It is conjectured that sparseness constraints imposed on either mixing vector or source image ensured physically sensible solution. This is illustrated by blind deconvolution of blurred image where algorithm has been run 100 times under different initial conditions for mixing vector and source image. Practically the same restored image has been obtained for every run. Extensive experimental comparative performance evaluation between novel non-negative matrix factorization algorithm and other representative blind and non-blind image deconvolution algorithms was presented. All image deconvolution methods were compared on images degraded by photon sieve, out-of-focus blur and atmospheric turbulence. It has been demonstrated that novel blind image deconvolution algorithm outperforms other methods. We conjecture that this result is due to the fact that SFNMF algorithm does not require any *a priori* information about the blurring kernel and original image.

Acknowledgements

The authors thank the Army Research Laboratory for their generous support of this research. This material is based upon work supported in part by the Army Research Laboratory under Cooperative Agreement W911NF-04-2-0035 and the Army Research Office under Contract No. W911NF-04-C-1236. Any opinions, findings and conclusions or recommendations expressed in this material are those of the authors and do not necessarily reflect the views of the Army Research Laboratory or the Army Research Office.

References

[1] M.R. Banham, A.K. Katsaggelos, IEEE Signal Process. Mag. 14 (1997) 24.
[2] D. Kundur, D. Hatzinakos, IEEE Signal Process.Mag. 13 (1996) 43.
[3] W.H. Richardson, J. Opt. Soc. Am. 62 (1972) 55.
[4] L.B. Lucy, Astron. J. 79 (1974) 745.
[5] D.A. Fish, A.M. Brinicombe, E.R. Pike, J.G. Walker, J. Opt. Soc. Am. A 12 (1995) 58.
[6] D.S.C. Biggs, M. Andrews, Appl. Opt. 36 (1997) 1766.
[7] M.M. Bronstein, A. Bronstein, M. Zibulevsky, Y.Y. Zeevi, IEEE Trans. Image Process. 14 (2005) 726.
[8] A. Hyvärinen, J. Karhunen, E. Oja, Independent Component Analysis, Wiley Interscience, 2001.
[9] I. Kopriva, Q. Du, H. Szu, W. Wasylkiwskyj, Opt. Commun. 233 (2004) 7.
[10] S. Umeyama, Scripta Technica, Electron. Comm. Jpn., Pt. 3 (84) (2001) 1.
[11] J.G. Daugman, IEEE Trans. Acoust., Speech Sig. Proc. 36 (1988) 1169.
[12] M. Numata, N. Hamada, in: Proceedings of 2004 RISP International Workshop on Nonlinear Circuit and Signal Processing (NCSP'04), 2004, p. 197.
[13] I. Kopriva, Opt. Lett. 30 (2005) 3135.
[14] R.L. Lagendijk, J. Biemond, Iterative Identification and Restoration of Images, KAP, 1991.
[15] H.H. Barrett, K.J. Myers, Foundations of Image Science, John Wiley, 2004.
[16] R. Molina, J. Nunez, F.J. Cortijo, J. Mateos, IEEE Signal Process. Mag. 18 (2001) 11.
[17] E.S. Meinel, JOSA A. 3 (1986) 787.
[18] A.R. De Pierro, Multiplicative iterative methods in computed tomography, in: G.T. Herman, A.K. Louis, F. Natterer (Eds.), Mathematical Methods in Tomography, Springer-Verlag, 1990.
[19] P.O. Hoyer, J. Mach. Learning Res. 5 (2004) 1457.
[20] D.D. Lee, H.S. Seung, Nature 401 (6755) (1999) 788.
[21] A. Cichocki, S. Amari, R. Zdunek, Z. He, R. Kompass, in: Proceedings of Eighth International Conference on Artificial Intelligence and Soft Computing, ICAISC, Zakopane, Poland, 25–29 June, 2006.
[22] A. Cichocki, R. Zdunek, S. Amari, Lecture Notes Comput. Sci. 3889 (2006) 32.
[23] Y. Li, A. Cichocki, S. Amari, Neural Comput. 16 (2004) 1193.
[24] Y. Li, S. Amari, A. Cichocki, D.W.C. Ho, S. Xie, IEEE Trans. Signal Process. 54 (2006) 423.
[25] A. Hyvärinen, E. Oja, Neural Comput. 9 (1997) 1483.
[26] J.F. Cardoso, A. Souloumiac, IEE-Proc. F 140 (1993) 362.